Front. Struct. Civ. Eng. 2020, 14(2): 532–553
https://doi.org/10.1007/s11709-020-0604-9

RESEARCH ARTICLE

Large deflection behavior effect in reinforced concrete columns exposed to extreme dynamic loads

Masoud ABEDINI[a*], Azrul A. MUTALIB[b*], Chunwei ZHANG[a*], Javad MEHRMASHHADI[c], Sudharshan Naidu RAMAN[d], Roozbeh ALIPOUR[e], Tohid MOMENI[e], Mohamed H. MUSSA[b]

[a] *School of Civil Engineering, Qingdao University of Technology, Qingdao 266033, China*

[b] *Department of Civil and Structural Engineering, Universiti Kebangsaan Malaysia, UKM Bangi, Selangor 43600, Malaysia*

[c] *Department of Mechanical and Materials Engineering, University of Nebraska-Lincoln, Lincoln, NE 68588, United States*

[d] *Department of Architecture and Built Environment, Universiti Kebangsaan Malaysia, UKM Bangi, Selangor 43600, Malaysia*

[e] *Department of Mechanical Engineering, Mahshahr Branch, Islamic Azad University, Mahshahr, Iran*

[*] *Corresponding authors. E-mails: m.abedini@qut.edu.cn; azrulaam@ukm.edu.my; zhangchunwei@qut.edu.cn*

ABSTRACT Reinforced concretes (RC) have been widely used in constructions. In construction, one of the critical elements carrying a high percentage of the weight is columns which were not used to design to absorb large dynamic load like surface bursts. This study focuses on investigating blast load parameters to design of RC columns to withstand blast detonation. The numerical model is based on finite element analysis using LS-DYNA. Numerical results are validated against blast field tests available in the literature. Couples of simulations are performed with changing blast parameters to study effects of various scaled distances on the nonlinear behavior of RC columns. According to simulation results, the scaled distance has a substantial influence on the blast response of RC columns. With lower scaled distance, higher peak pressure and larger pressure impulse are applied on the RC column. Eventually, keeping the scaled distance unchanged, increasing the charge weight or shorter standoff distance cause more damage to the RC column. Intensive studies are carried out to investigate the effects of scaled distance and charge weight on the damage degree and residual axial load carrying capacity of RC columns with various column width, longitudinal reinforcement ratio and concrete strength. Results of this research will be used to assessment the effect of an explosion on the dynamic behavior of RC columns.

KEYWORDS RC column, scaled distance, blast load, LS-DYNA

1 Introduction

Traditionally, reinforced concrete (RC) columns were designed to withstand only gravity loads. With time and improved analytical tools, seismic activity was included in the design as well. Recently, the susceptibility of columns to transverse loadings caused by extreme shocks, such as impacts and explosions, has garnered increasing attention [1]. An RC column may be subjected to different loading conditions such as static, dynamic, or short-duration dynamic loads. Generally, static loads are considered time-independent since they do not produce inertia effect and may last very long such as gravity compared to dynamic loads [2]. Dynamic loads may be referred to earthquake loads or wind gusts as time-dependent loads. However, short-term dynamic loads like load caused by explosive are of order 10^{-2} s which are approximately one thousand times shorter than earthquake periods [3]. Figure 1 provides an example of different dynamic hazards with their respective amplitude-frequency relationships.

Some researchers have already studied the behavior of RC columns under surface burst [4–8]. Blast parameters which change the RC performance are the shape of structures and geometries, standoff distance, the part of the structure facing toward the blast load, and the opening of the structures [9–11]. Ngo et al. [12] claimed two most important parameters describing the severity of the damage are standoff distance and the charge weight. Almusallam et al. [13] studied the blast performance of an eight-story building framed with RC structure. He showed those

Article history: Received Jan 6, 2019; Accepted Mar 15, 2019

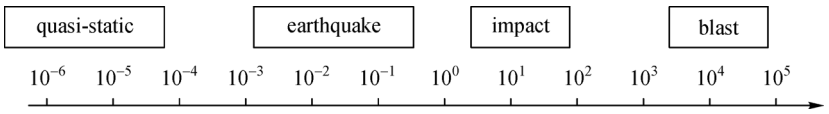

Fig. 1 An estimation to strain rates caused by different types of loading.

columns experiencing reflected pressure as they were placed toward the blast waves, received the most damage. Steel bars in those columns were damaged, and the concrete fragmented. Consequently, with no load-bearing capacity, the gravity loads initiated some partial collapse. Remennikov [14] compared some analytical approach with numerical techniques to predict blast loads. He determined the limitation and simulated a simple explosion test. Calculating the blast pressure using UFC standard allowed Remennikov to apply directly to the structure [15]. He modeled the structure but not air nor the charge. Simulation with no air elements was very computationally efficient and required less time. Baylot and Bevins [16] conducted an investigation on a RC column subjected to blast loads. The study consisted of both experimental and numerical approaches, and reports including modelling details of structural configurations and experimentally observed results at various locations of the RC models.

This work focuses on investigating the effect of blast variables on RC columns. In this research finite element analysis and validation of experimental field test are investigated for RC columns when subjected to blast detonation. Parametric studies are accomplished to examine the consequence of scaled distance on RC columns against explosive loadings.

2 Preparing the finite element model

The Numerical model of the RC column with the height 4.4 m, the cross section of 500 mm × 700 mm including eight longitudinal reinforcements of ϕ25 mm and transverse reinforcement of ϕ12 mm is modeled in LS-DYNA. Bars are meshed with Hughes-Liu beam elements with 2 × 2 Gauss integration (see Fig. 2), and the concrete is meshed with constant stress solid elements of size 50 mm [17]. RC column is constrained on both ends except the vertical degrees of freedom of nodes on top of the column which are free. These nodes are subjected to an axial load. Material properties are listed in Table 1. Detail description of the RC column are represented in Fig. 3.

Table 1 Concrete and steel reinforcement properties

material	parameters	value
concrete	uniaxial compressive strength	42 MPa
	mass density	2400 kg/m^3
	Poisson's ratio	0.2
	tensile stress at failure	6.0 MPa
steel reinforcement	Young's modulus	200 GPa
	longitudinal steel strength	460 MPa
	transverse steel strength	250 MPa
	mass density	7800 kg/m^3
	Poisson's ratio	0.3
	plastic strain at failure	0.18

2.1 Material models

LS-DYNA provided a comprehensive material database covering different concrete behavior. Concrete may act ductile under hydrostatic pressure or may act brittle under tensile loads like explosive loads [19,20]. The concrete is

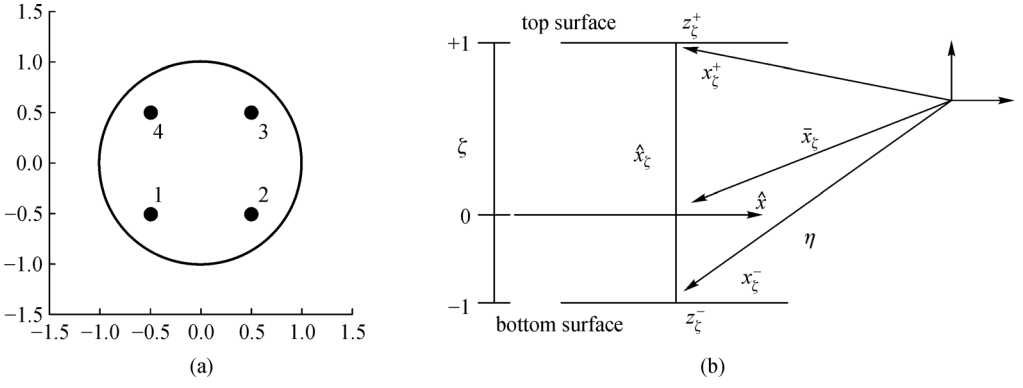

Fig. 2 (a) Integration possibilities for circular cross sections; (b) Hughes-Liu beam element (LS-DYNA Manual).

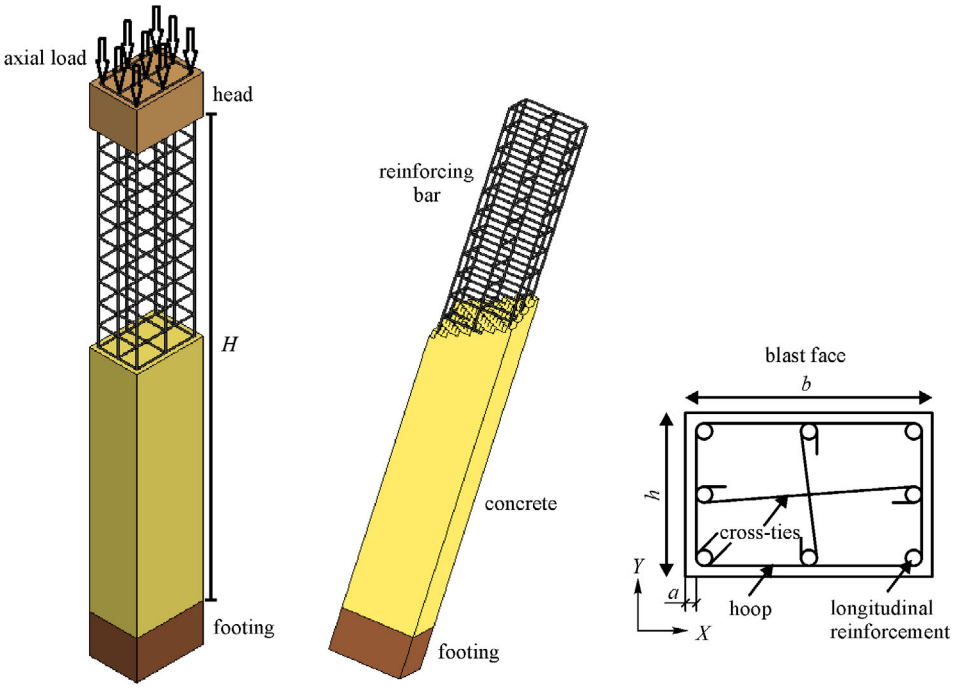

Fig. 3 Detail description of the RC column.

modeled with *MAT-CONCRETE-DAMAGE-REL3 which requires only the unconfined compressive strength in the calibration process [21,22]. The Karagozian & Case Concrete Model is a three-invariant model which uses a three-parameter function to represent the variation of compressive shear strength with mean stress of the form shown in Eq. (1). This material model also includes damage and strain-rate effects.

$$SD = a_0 + \frac{P}{a_1 + a_2 P'}, \tag{1}$$

where SD is the stress difference and P is the mean stress in a triaxial compression failure test, and the parameters (a_0,a_1,a_2) are determined by a regression fit of Eq. (1) to the available laboratory data. Table 2 shows concrete material properties where ρ is mass density, f_c is concrete strength, and v is Poisson's ratio. The material of rebars is considered as material type 24 shown in Table 3 where E is Young's Modulus, f_y is longitudinal steel strength, and f_{yt} is transverse steel strength [17,23].

Table 2 The concrete material properties

parameter	ρ	f_c	v
value	2400 kg/m^3	42 MPa	0.2

LS-DYNA provided the keyword of *MAT_ADD_EROSION to delete those elements meeting erosion criterion [19]. This keyword adds erosion criterion to materials which do not have any failure criteria. Although this keyword helps to understand the failure mechanism, it also affects the mass and the inertia properties of the model by removing elements. Therefore, using this keyword is only suggested to investigate the damage mechanism graphically. A number of criterions are available in LS-DYNA for this keyword. We used the maximum effective strain at failure shown in Eq. (2) is used for this studied.

$$\varepsilon_{\text{eff}} = \sum_{ij} \sqrt{\frac{2}{3} \varepsilon_{ij}^{\text{dev}} \varepsilon_{ij}^{\text{dev}}}, \tag{2}$$

where $\varepsilon_{ij}^{\text{dev}}$ is the deviatoric strain states.

Among those various methods available in the literature, peridynamics as a nonlocal form of continuum mechanics has increasingly used to study fracture and crack propagation in many fields and has been validated against a variety of experimental tests [24–29]. In peridynamics, the damage is a part of the solution not a part of the problem. However, peridynamic (PD) modeling of RC column requires a dense grid, and the stable timestep in the explicit integration would be relatively low for the current

Table 3 Material properties of rebars

parameter	ρ	E	v	f_y (longitudinal rebars)	f_{yt} (transverse rebars)
value	7800 kg/m^3	200 GPa	0.3	450 MPa	400 MPa

study [30]. Therefore, PD modeling of the RC column might not be computationally efficient.

2.2 Strain rate

Higher strain rate can sometimes increase the strength of the material. This behavior is identified as the dynamic increase factor (*DIF*). Tensile *DIF* (*TDIF*) is a function of tensile strengths at high strain rate and tensile strength at static loadings. Similarly, Compressive *DIF* (*CDIF*) represents compressive strengths at high strain rate versus compressive strength at static loadings. To investigating the effect of high strain rate loads such explosive on the behavior of the RC column, *DIF* is calculated for each type of loading and is applied directly to the material model.

2.2.1 Modified strain rate for concrete in compression

Many researchers have studied the influence of high strain rate on the behavior of concrete materials. Watstein [31], Jones and Richart [32], and Glanville et al. [33] showed that the increase of loading rate also increased the compressive strength of the concrete. For a strain rate of 10 s^{-1}, Watstein [31] recommended an increase of 80% in compressive strength. DIF for the compressive strength of the concrete was formulated using the CEB-FIB Model Code [34] as follows:

$$CDIF = \frac{f_c}{f_{cs}} = \left[\frac{\dot{\varepsilon}}{\dot{\varepsilon}_{cs}}\right]^{1.026\alpha}, \text{ for } \dot{\varepsilon} \leqslant 30\, s^{-1}, \tag{3}$$

$$CDIF = \frac{f_c}{f_{cs}} = \gamma\left(\frac{\dot{\varepsilon}}{\dot{\varepsilon}_{cs}}\right)^{\frac{1}{3}}, \text{ for } \dot{\varepsilon} > 30\, s^{-1}, \tag{4}$$

$$\log\gamma = 6.15\alpha - 0.49, \tag{5}$$

$$\alpha = \frac{1}{5 + \frac{3f_{cu}}{4}}, \tag{6}$$

where f_{cd} = compressive strength (dynamic) at $\dot{\varepsilon}$, f_{cs} = compressive strength (static) at $\dot{\varepsilon}_{cs}$, *CDIF* = compressive *DIF*, f_{cu} = static cube strength, $\dot{\varepsilon}_{cs} = 3 \times 10^7\, s^{-1}$ (static strain rate), f'_{co} = 10 MPa, $\dot{\varepsilon}$ = strain rate ($3 \times 10^7 - 300\, s^{-1}$).

2.2.2 Modified strain rate for concrete in tension

Concrete is also sensitive to tensile strain rate due to the heterogeneity of the material [35]. Tensile strength can be increased a substantial amount for loading rates beyond 10 MPa/s. Tensile *DIF* for a given strain rate may be estimated from the following equations.

$$TDIF = \frac{f_t}{f_{ts}} = \left[\frac{\dot{\varepsilon}}{\dot{\varepsilon}_{ts}}\right]^{\delta}, \text{ if } \dot{\varepsilon} \leqslant 1\, s^{-1}, \tag{7}$$

$$TDIF = \frac{f_t}{f_{ts}} = \beta\left[\frac{\dot{\varepsilon}}{\dot{\varepsilon}_{ts}}\right]^{\frac{1}{3}}, \text{ if } \dot{\varepsilon} > 1\, s^{-1}, \tag{8}$$

$$\beta = 7.11\delta - 2.33, \tag{9}$$

$$\delta = \frac{1}{10 + \frac{6f'_t}{f_{co}}}, \tag{10}$$

where $\dot{\varepsilon}$ = strain rate ($3 \times 10^{-6} - 300\, s^{-1}$), $\dot{\varepsilon}_{ts} = 3 \times 10^{-6}\, s^{-1}$ (static strain rate), f'_{co} = 10 MPa, f_{ts} = tensile strength (static) at $\dot{\varepsilon}_{ts}$, f_t = tensile strength (dynamic) at $\dot{\varepsilon}$, f'_c = static uniaxial strength of concrete (in MPa).

2.2.3 Modified strain rate for steel

The sensitivity of stress and strain curves of steels to loading rates is called the strain rate sensitivity [36,37]. Strain rate sensitivity has a important consequence on the inertia effect of the material and affects the load-displacement curve tested under different uniaxial compression strain rates [38,39]. Malvar introduced DIF as the new equation for steel ASTM rebars which represented the effect of strain rate on the strength improvement [40]. Malvar leveraged test results available in the literature to derive his equation as follows:

$$DIF = \frac{(\dot{\varepsilon})^{\alpha}}{10^{-4}}, \tag{11}$$

$$\alpha = 0.019 - 0.009\frac{f_y}{414}, \text{ for ultimate stress}, \tag{12}$$

$$\alpha = 0.074 - 0.040\frac{f_y}{414}, \text{ for yield sress}, \tag{13}$$

where f_y = steel yield stress.

2.3 Contact algorithm

In this study, the keyword of CONTACT_1D is implemented to consider the bond-slip interactive effect between the concrete and longitudinal rebars [41]. The bond between the rebar and concrete is assumed to be elastic perfectly plastic. The maximum allowable slip strain is given as:

$$\mu_{max} = \text{SMAX} \times e^{-\text{EXP}\times D}, \tag{14}$$

where D is the damage parameter $D_{n+1} = D_n + \Delta u$. The shear force, acting on area A_s, at time $n + 1$ is given as:

$$f_{n+1} = \min[f_n - GB \times A_s \times \Delta u, GB \times A_s \times u_{max}], \quad (15)$$

where GB is bond shear modulus and SMAX is the maximum shear strain. This contact algorithm makes steel nodes dependent on concrete nodes and allows stress transfer between different materials. The stress transfer can affect the dynamic behavior of the RC column [42,43]. Methods considering perfect bond assumption have been previously used by researchers such as Fanning [44], and Tavárez [45]. In this method, steel nodes are merged into concrete nodes. Consequently, the failure criterion for the steel material would entirely depend on the failure of the concrete.

3 Simulation of explosive load in LS-DYNA

Several ways can be used to simulate explosive loads in LS-DYNA considering explicit integration [30]. The simplest method is computing the time history of the blast pressure at the point of interest from other source and then apply the pressure directly on the structure [46]. The idealized pressure profile can be of the triangular ramped form (see Fig. 4) applied uniformly on the front face [47]. The keyword of LOAD_SEGMENT_SET is used to define the pressure profile and column front surface [48]. Although the reflected pressure and pressure superposition near the front face are neglected, this approach can qualitatively capture the failure mechanisms of RC columns subjected to surface burst and to reveal the effectiveness of the multi-hazard detailing on the blast resistance of ordinary highway bridges. Compared to other blast load techniques, the pressure time history method offers computational time savings.

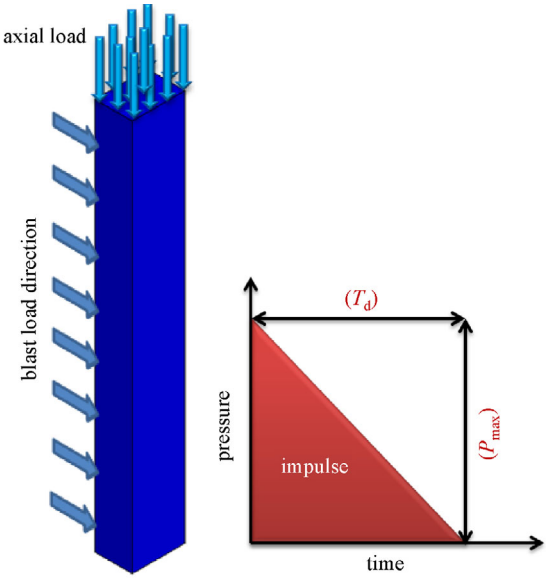

Fig. 4 Simplified blast pressure-time method.

4 Verification of numerical models

The proposed numerical model is validated against Baylot's and Benvis' experiment No.02 which investigated the behavior of the exterior middle column [16]. The dimensions of the column were: the cross-section of 85 mm × 85 mm, span length of 0.935 m, eight longitudinal rebars of ϕ7 mm, and stirrups of ϕ3.5 mm which closed longitudinal reinforcements. Material properties of the column were: unconfined concrete strength of 42 MPa, ρ = 2068 kg/m^3, and E = 28.7 GPa. Material properties of rebars were: yield stress of 450 and 400 MPa for longitudinal and transverse reinforcement, respectively. Charge weight of 7.087 kg C4 was placed at the standoff distance of 1.07 m and 228.6 mm above the ground (see Fig. 5). Baylot and Bevins [16] provided finite element analyses in addition to their experiments. The sequence of effective plastic strain variations available in the CONCRETE_DAMAGE_REL3 material model as damage parameter is illustrated in Fig. 6. Colors show the level of concrete damage. The blue color denotes no damage, the red color represents the residual capacity of the concrete, and other colors represent the damage levels of the concrete.

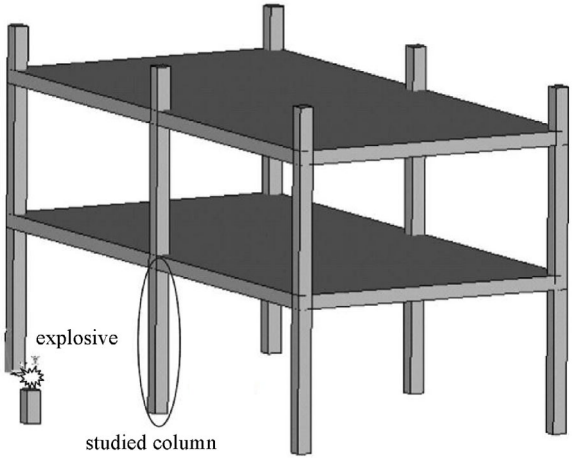

Fig. 5 Schematic view of column position.

The variation of the lateral displacement at mid-height of the column is compared with the experiment (see Fig. 7). The horizontal displacement at the mid-height was 12.5 and 12 mm in experiment and the present study, respectively. The difference in the lateral deflection was only about 4.16%. However, residual deflections are almost the same in both present analysis and experimental results (6.3 mm). In conclusion, the presented finite element model is validated using experimental data obtained by Baylot and Bevins [16].

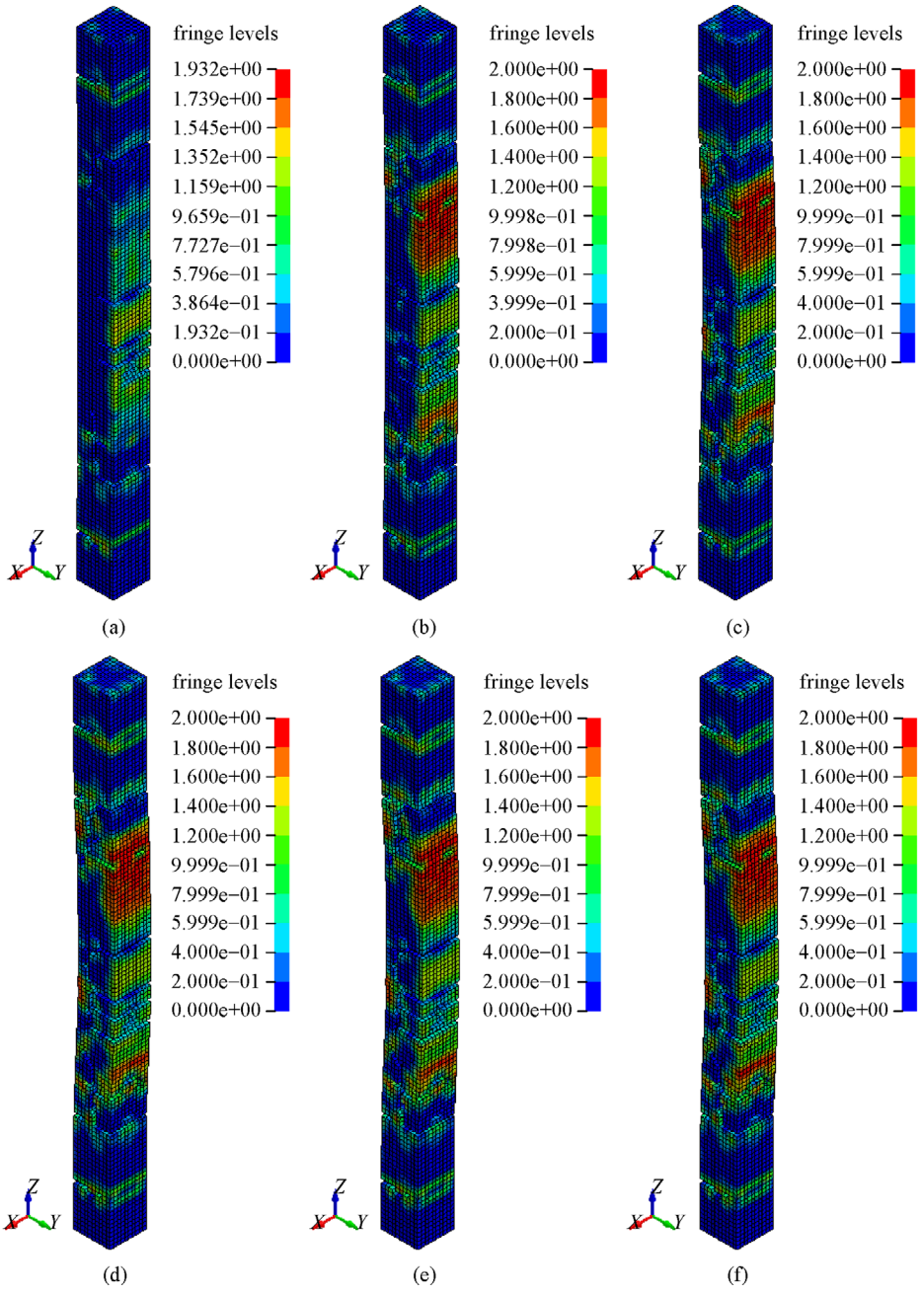

Fig. 6 Plots of effective strain diagrams at different times. (a) $t = 10$ ms; (b) $t = 11$ ms; (c) $t = 12.5$ ms; (d) $t = 14.5$ ms; (e) $t = 15.5$ ms; (f) $t = 16.5$ ms.

5 Numerical analysis

Structural response exposed to explosive loads can be classified based on the strength of the explosive pressure called high/low pressure. Scaled distance (Z) defines the intensity of the blast pressure and is defined as the ratio of standoff distance and the cube root of the charge weight [49]. The target designed to stand against the high-pressure waves is typically placed near the charge and absorbs reflected pressure whereas, targets designed for low-pressure range are often experience the side on pressure and are mostly positioned parallel to wave propagation [49]. Blast parameters for any blast event are found as functions of the distance from the blast center (R) and the equivalent charge weight (W). Scaled distance is of the following form:

$$Z = \frac{R}{W^{1/3}}. \tag{16}$$

Three regimes are defined by Smith et al. [50] using Z

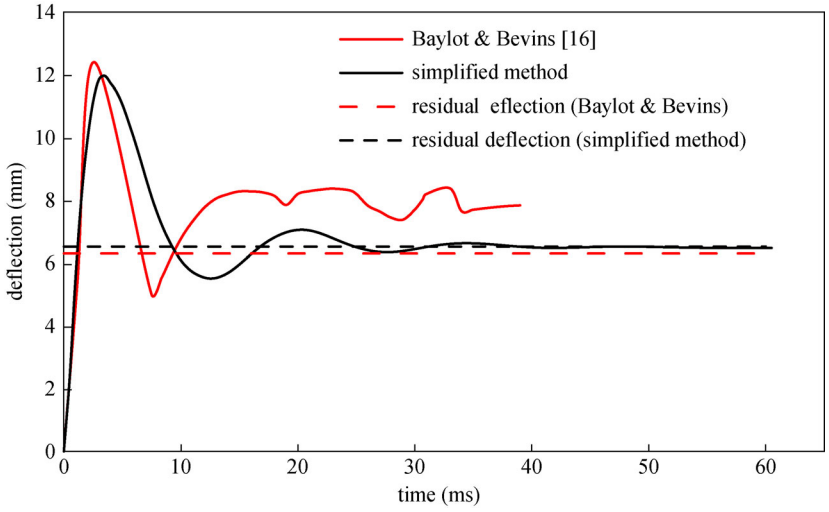

Fig. 7 Deflection time histories of mid-height [16].

shown in Table 4. Scaled distances corresponding to the charge mass of 100 kg and three standoff distances are calculated using Eq. (16) and presented in Table 5.

Table 4 Categories of response regime [50]

scaled distance	Z (m/kg$^{1/3}$)	Z (ft./lb$^{1/3}$)
close-in	$Z<1.190$	$Z<3$
near-field	$1.190<Z<3.967$	$3<Z<10$
far-field	$Z>3.967$	$Z>10$

Table 5 Scaled distances at 100 kg charge weight subjected to close-in, near-field, and far-field detonation

regimes of blast load	standoff distance (m)	charge weight (kg)	scaled distance (m/kg$^{1/3}$)
close-in	2.79	100.0	0.6
	3.71		0.8
	4.64		1.0
near-field	6.96	100.0	1.5
	9.28		2.0
	11.60		2.5
far-field	18.56	100.0	4.0
	20.88		4.5
	23.20		5.0

6 Results and discussion

6.1 The RC column behavior under various scaled distances

A series of simulations were conducted to observe the response of the RC columns subjected to explosive load variations. Maximum and minimum principle stress graphs can be used to measure the performance of RC columns during the extreme load conditions. In this section the minimum and maximum principal stress graphs generated from selected elements at critical locations of RC columns. The scaled distance for selected column is 0.6 m/kg$^{1/3}$. A cross section was captured at middle height of the RC column as shown in Figs. 8(a) and 8(b) demonstrates the cross sectional behavior with selected elements with effective plastic strain.

Figures 9 and 10 show stress plots for elements selected from middle and one side of the column along the blast direction. In the Fig. 9, stress values at elements 7134 and 7064 are very close, and hence the graphs coincide. As can be seen in Figs. 9 and 10, the elements in the selected column have been subjected to either tensile or compression failure and have completely lost their load carrying capacity as their principal stresses have become zero immediately after the blast. These stresses resulted in bond and adhesion failure between concrete and reinforcement and a loss of confinement of the concrete in the column.

Figure 11(a) shows the location of the weakest point of the column at scaled distance of 2 m/kg$^{1/3}$ and Fig. 11(b) shows the cross section of the effective undamaged concrete. The selected elements are used to assess the damage degree of RC columns when subjected to blast detonations. The section was captured at 15 ms of time history before progressive collapse started due to lack of load carrying capacity of the entire frame following the blast.

Maximum and minimum principal stress plots for selected particular elements in Fig. 11(b) are illustrated in Figs. 12 and 13. The elements number 7148 and 7141 lost their stress and could not carry any load immediately after the blast load imposed. The concrete elements 7274, 7204, 7267, and 7197 carried post blast gravity load as their principal stresses were not zero. The strain diagram

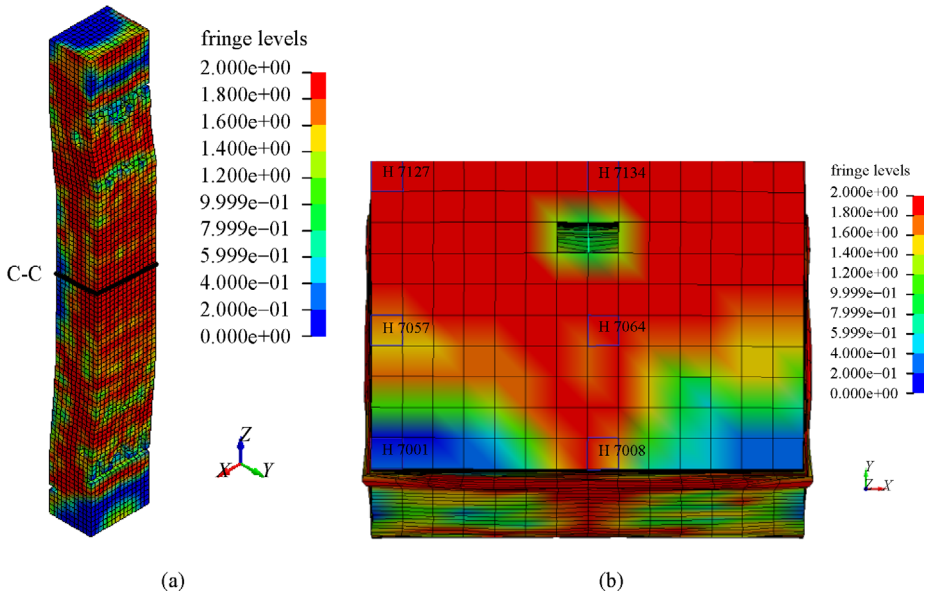

Fig. 8 (a) The cross section at mid-height of the column and (b) cross section C-C with selected elements in concrete.

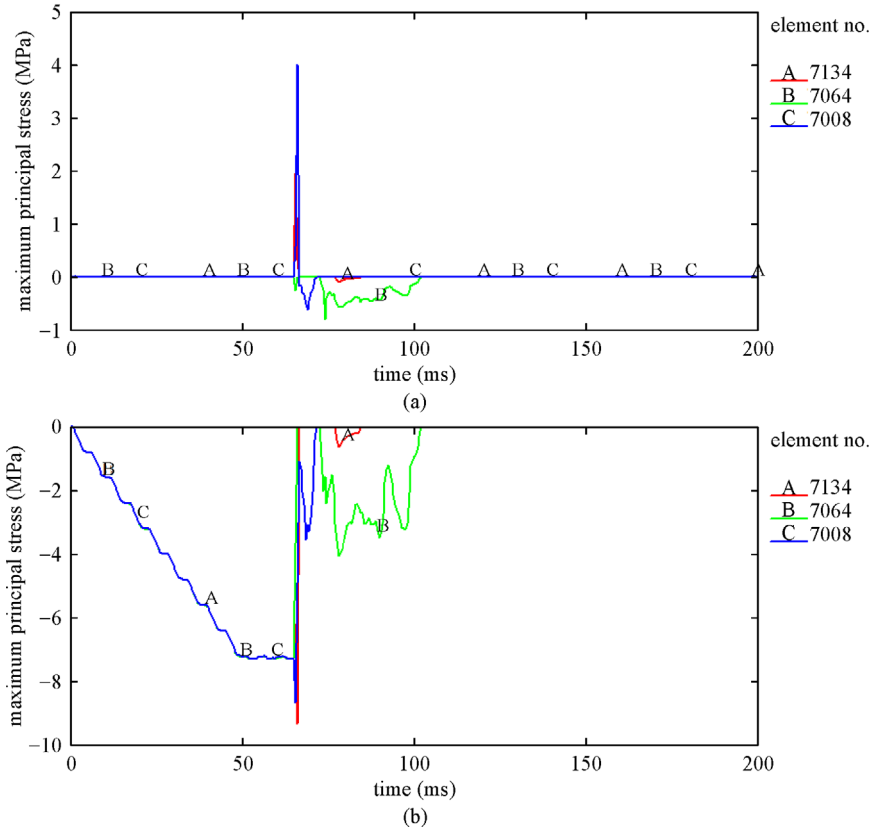

Fig. 9 (a) Maximum and (b) minimum principle stress plots for elements selected at the middle of the column cross section.

clearly shows that the concrete was not yielded and stress plots confirmed it. When the bond between reinforcement and concrete disintegrates, blast damage results in loosen of confinement of concrete. However, the concrete damaged area experienced that the steel reinforcement became ineffective and concrete returns to the unconfined state. As a result, the load carrying capacity of the column is significantly reduced. The residual capacity of the

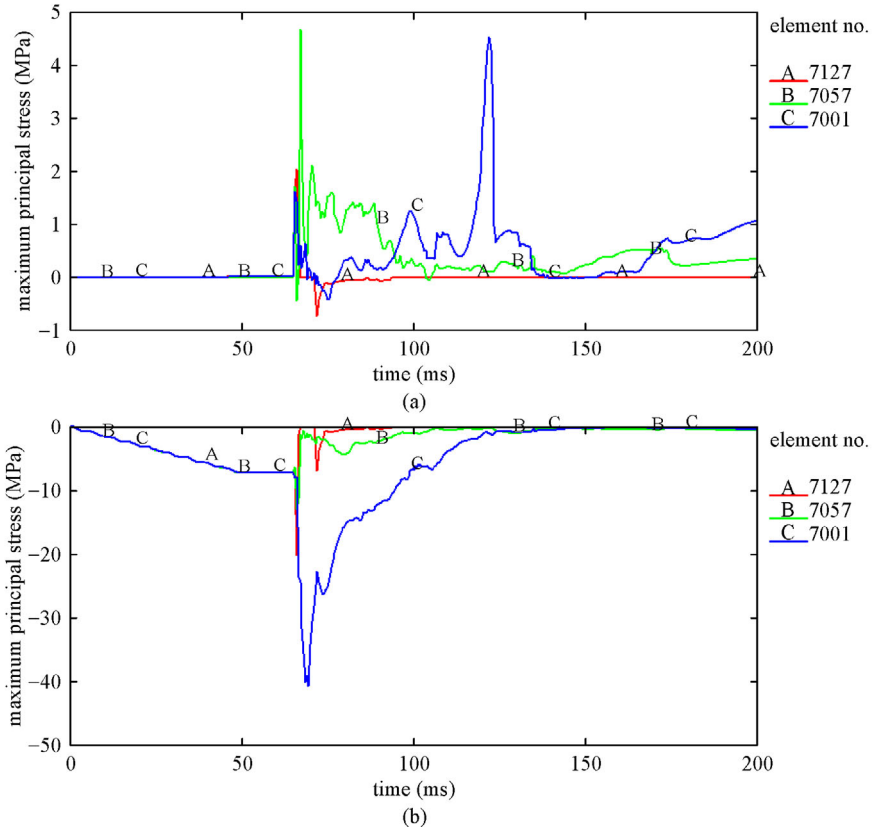

Fig. 10 (a) Maximum and (b) minimum principle stress plots for elements selected from one side of the column cross section.

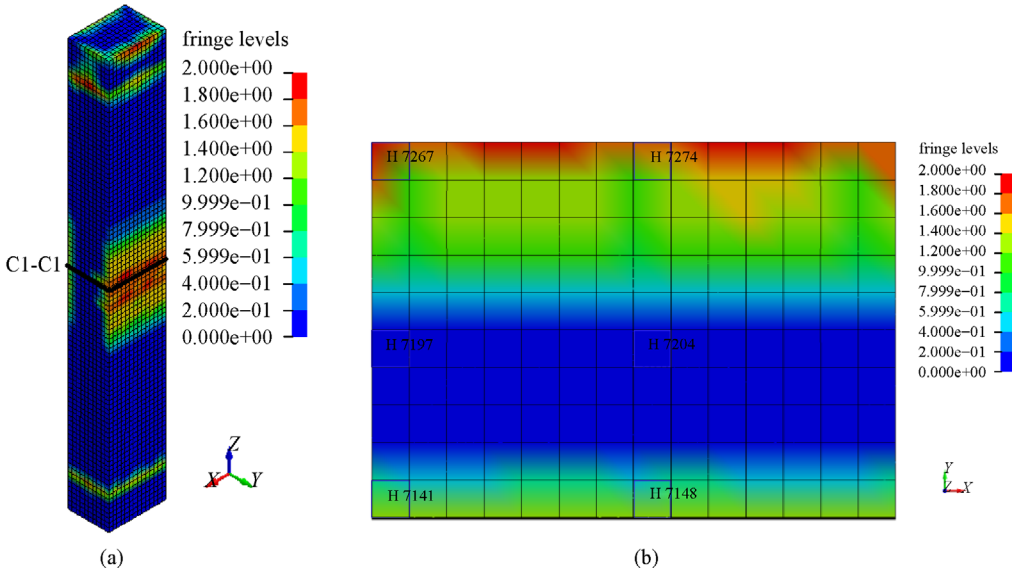

Fig. 11 (a) Selected cross section at weakest point of the column and (b) cross section C1-C1 with selected elements in concrete.

undamaged concrete can be calculated by evaluating the minimum cross-sectional area of effective undamaged concrete at the weakest point of the column.

Stress contour plots for different scaled distances under near-field, close-in, and far-field explosions are illustrated in Figs. 14–16. In the case of close-in detonations, the column lost their load carrying capacity and failed utterly. In case of near-field and far-field detonations, the column

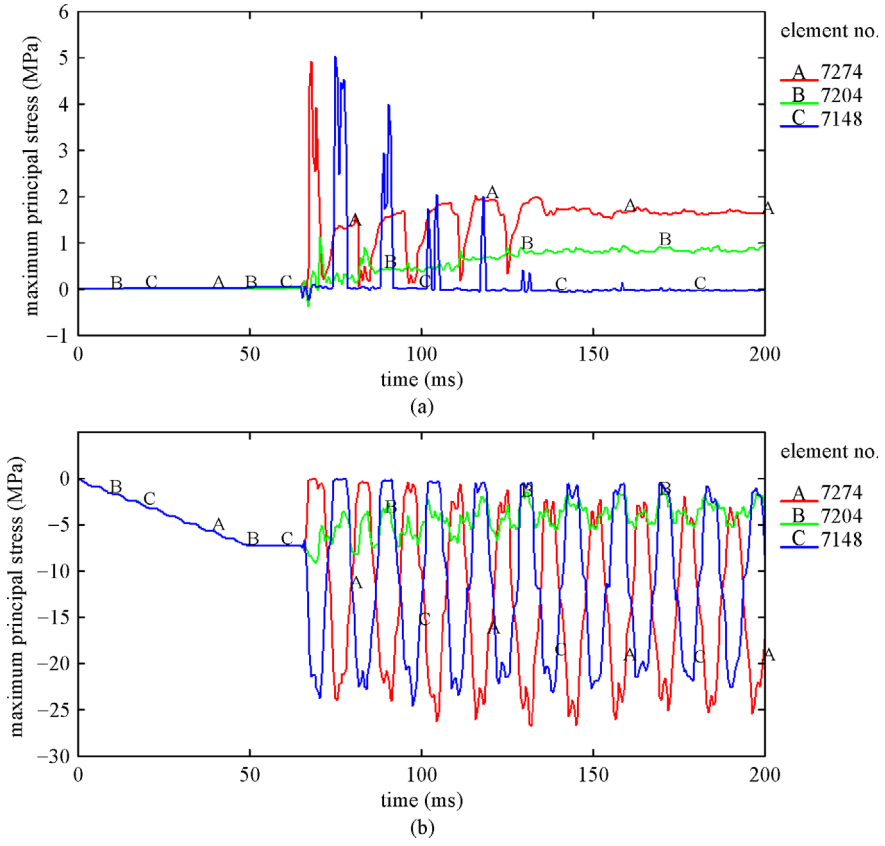

Fig. 12 (a) Maximum and (b) minimum principle stress plots for elements selected from middle of the column cross section.

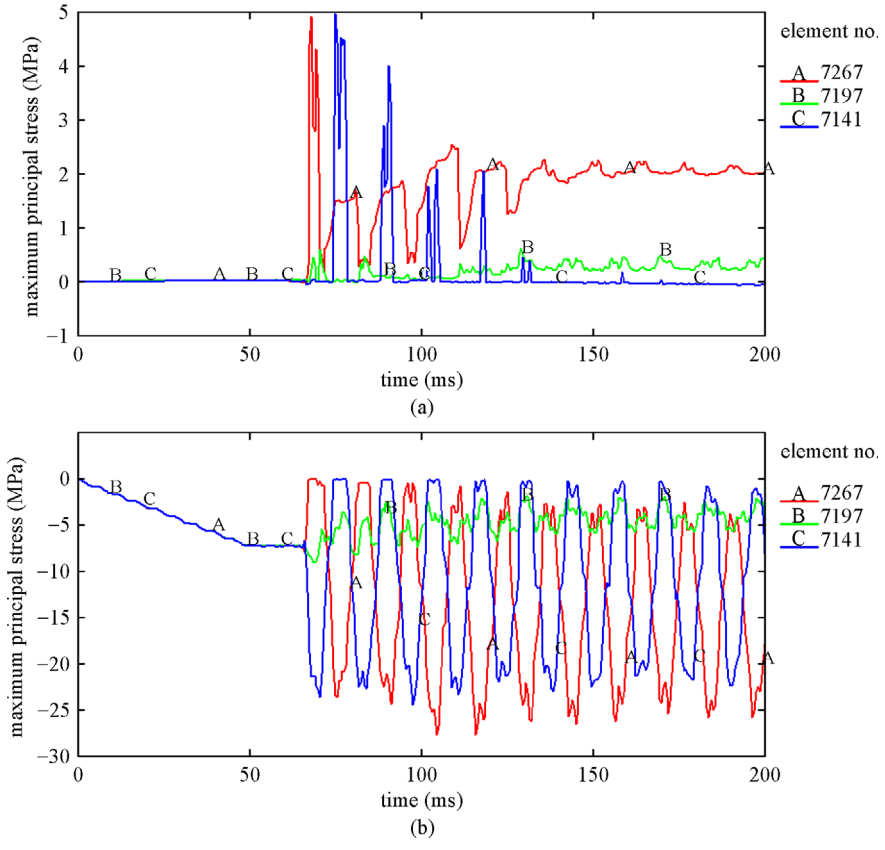

Fig. 13 (a) Maximum and (b) minimum principle stress plots for elements selected from one side of the column cross section.

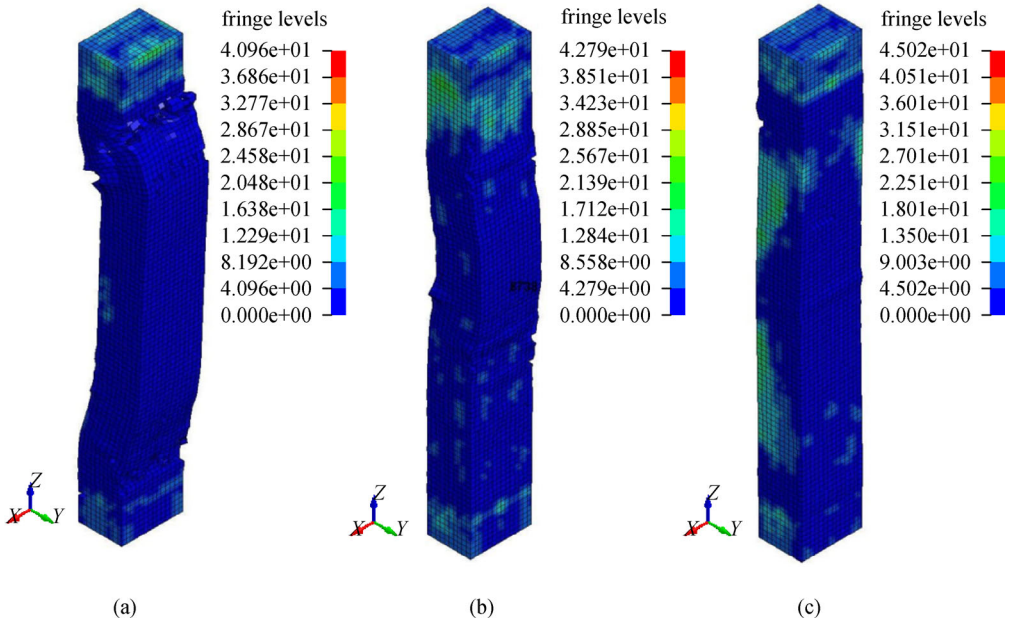

Fig. 14 Effective stress plots under close-in detonation. (a) $Z = 0.6$ m/kg$^{1/3}$; (b) $Z = 0.8$ m/kg$^{1/3}$; (c) $Z = 1$ m/kg$^{1/3}$.

remains undamaged and can sustain more blast loads as represents in Figs. 15 and 16. Results demonstrate that increasing the scaled distance significantly reduces the amount of damage to the structural system.

The peak pressure is incredibly intense in close-in detonation. In this case, the period of the blast wave is relatively shorter than the natural period of the column, and the column respond mainly to the impulse of the blast load as shown in Fig. 17. As a result, the impulse can be a better parameter than the peak pressure to design the target. According to Fig. 17, when the scaled distance is increased, the pressure and impulse in the RC column are decreased. In case of near-field, the response regime is called the dynamic regime and lies between the quasi-static and the impulsive regimes (see Fig. 18). For this regime, the period of the blast waves is almost the same as the natural period of vibration of the column. Simulation of these types of dynamic responses is complicated. How-

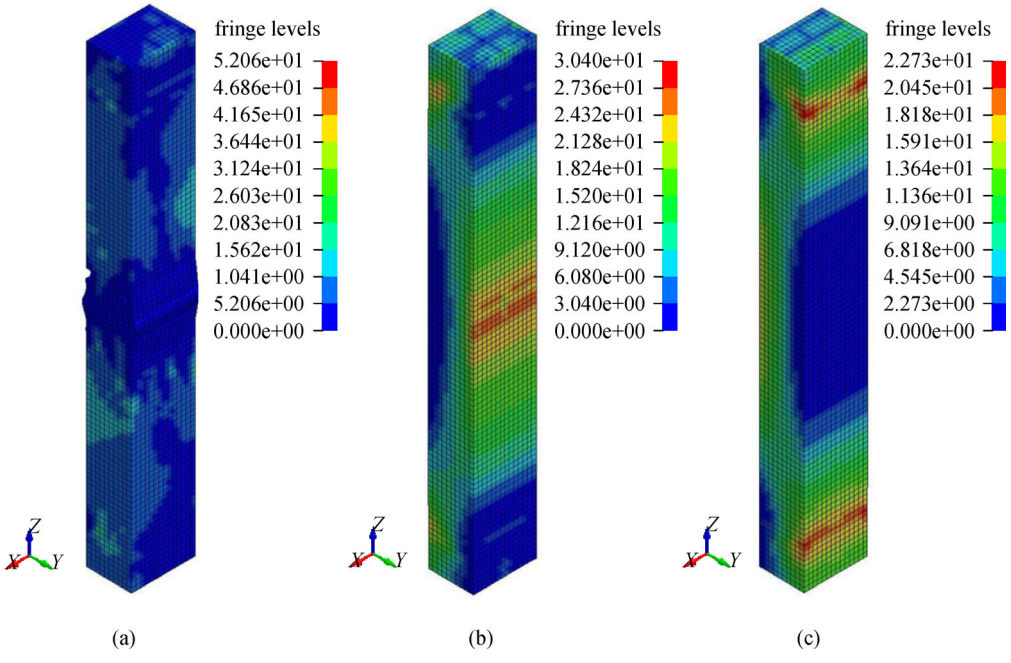

Fig. 15 Effective stress plots under near-field detonation. (a) $Z = 1.5$ m/kg$^{1/3}$; (b) $Z = 2$ m/kg$^{1/3}$; (c) $Z = 2.5$ m/kg$^{1/3}$.

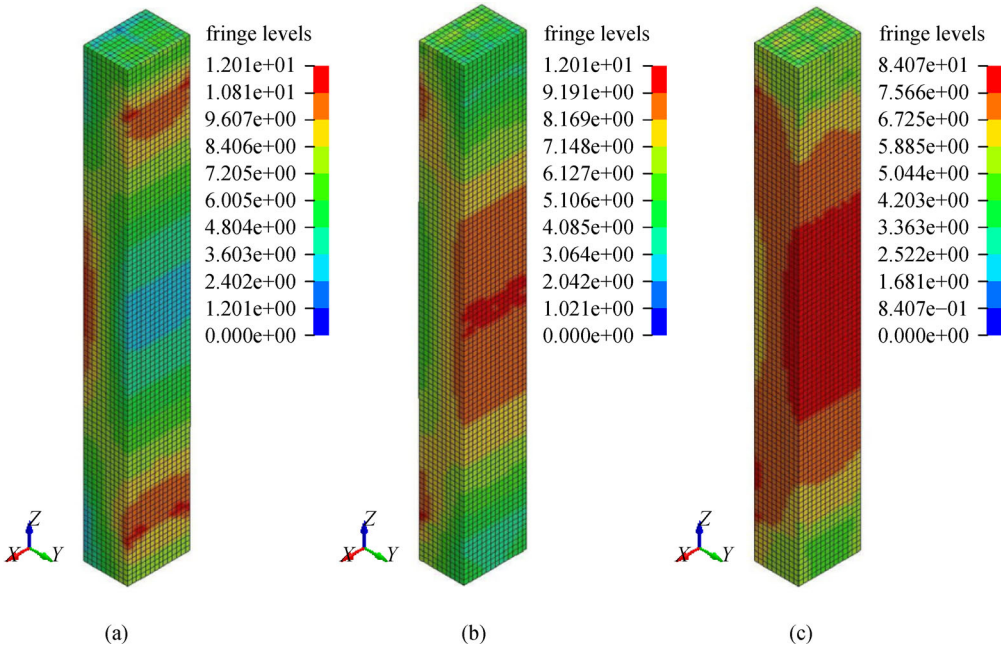

Fig. 16 Effective stress plots under far-field detonation. (a) $Z = 4$ m/kg$^{1/3}$; (b) $Z = 4.5$ m/kg$^{1/3}$; (c) $Z = 5$ m/kg$^{1/3}$.

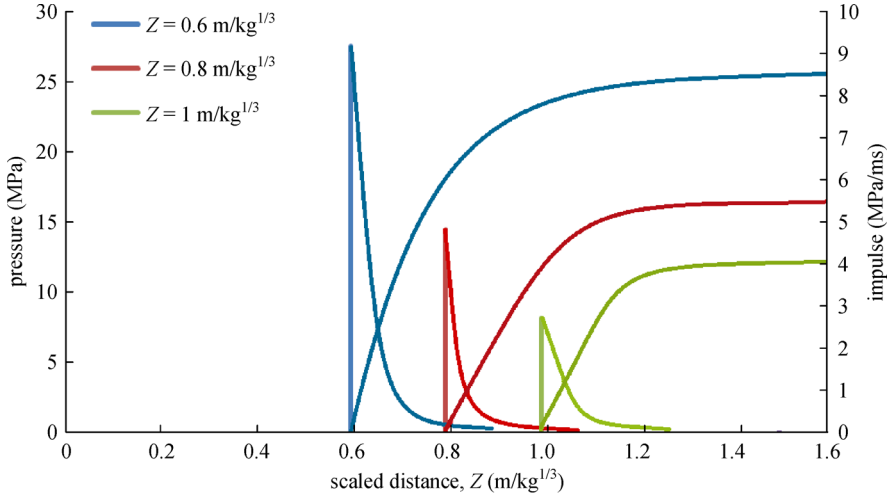

Fig. 17 Pressure and impulse graphs at different Z under close-in detonation.

ever, it is possible to approximate the response based on the impulsive and quasi-static cases. In case of far-field detonation, the peak pressure smaller than the one in the high-pressure range, impacts the RC column. Duration of the blast waves in far-field cases is remarkably more extended than the period of natural of the column shown in Fig. 19. Therefore, the explosive load can be considered as a quasi-static load. In a quasi-static load, the response of the structure is a function of applied load and may reach to the maximum deflection before the blast pressure drops. Hence, the maximum deflection depends on the peak pressure and structural stiffness.

Deflections of the RC column subjected to different scaled distances over 200 ms simulation are presented in Figs. 20–22. In the case of close-in detonation, the column fails due to the highly impulsive load. For such cases, significant structural deformations occur after the blast wave passed the structure. When the column is subjected to near-field detonations, the intensity of the blast loads reduced and the column sustain less blast damage as shown in Fig. 21. At a higher scaled distance, the lateral displacements decreased significantly in the near-field detonations range. When the column was under far-field detonation, the peak deflection recorded decreased in

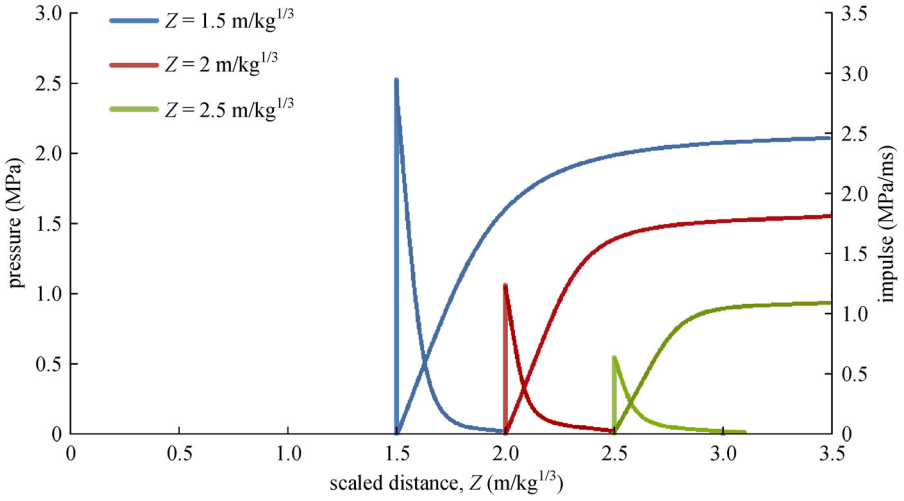

Fig. 18 Pressure and impulse graphs at different Z under near-field detonation.

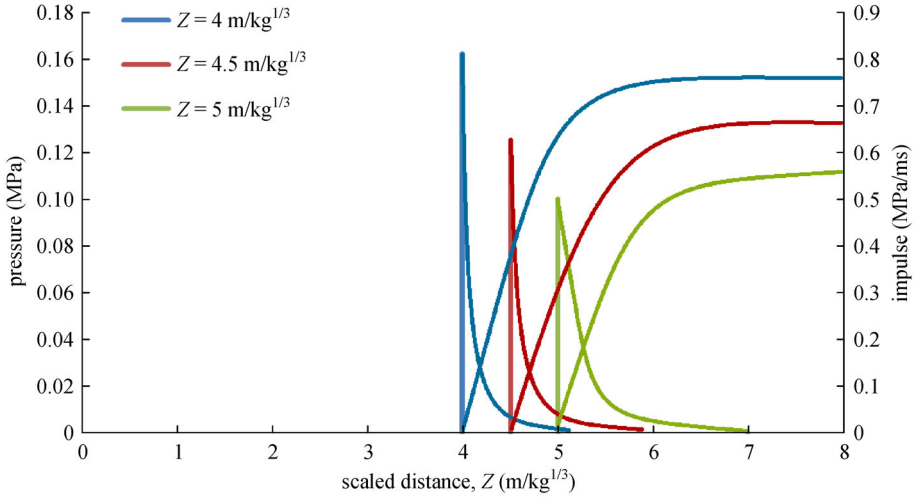

Fig. 19 Pressure and impulse graphs at different Z under far-field detonation.

comparison to near-field, and close-in detonations. Contour plots indicate less blast damage as represented in Fig. 22.

6.2 The response of the RC column under same scaled distance

The numerical analysis is extended to investigate the behavior of the RC column at Z = 0.95 m/kg$^{1/3}$ with different standoff distances and charge weights. In this section, the charge masses of 0.5, 5, 50, 597.2, 9330, and 15000 kg were used at the matching standoff distances of 0.753, 1.62, 3.5, 8, 20, and 23.58 m. Table 6 represents the range of charge weights and standoff distances at 0.95 m/kg$^{1/3}$. Figure 23 represents the dynamic behavior of the RC column under same scaled distance at 100 ms time. As the scaled distance is constant in Fig. 23, the level of damage increased with more charge weight and larger standoff distance. In this situation, the blast duration and blast impulse vary with different charge masses at the specific scaled distance. Heavier charges make longer blast loads. Therefore, at the same scaled distance, heavier charge produces higher impulse.

6.3 Influence of scaled distance on the damage degree of RC columns with different longitudinal reinforcement ratio

Numerical simulations were conducted to study the effect of scaled distance on the damage degree of RC columns with different longitudinal reinforcement ratio when subjected to explosive loads. The change in the longitudinal reinforcement ratio is accomplished by the change

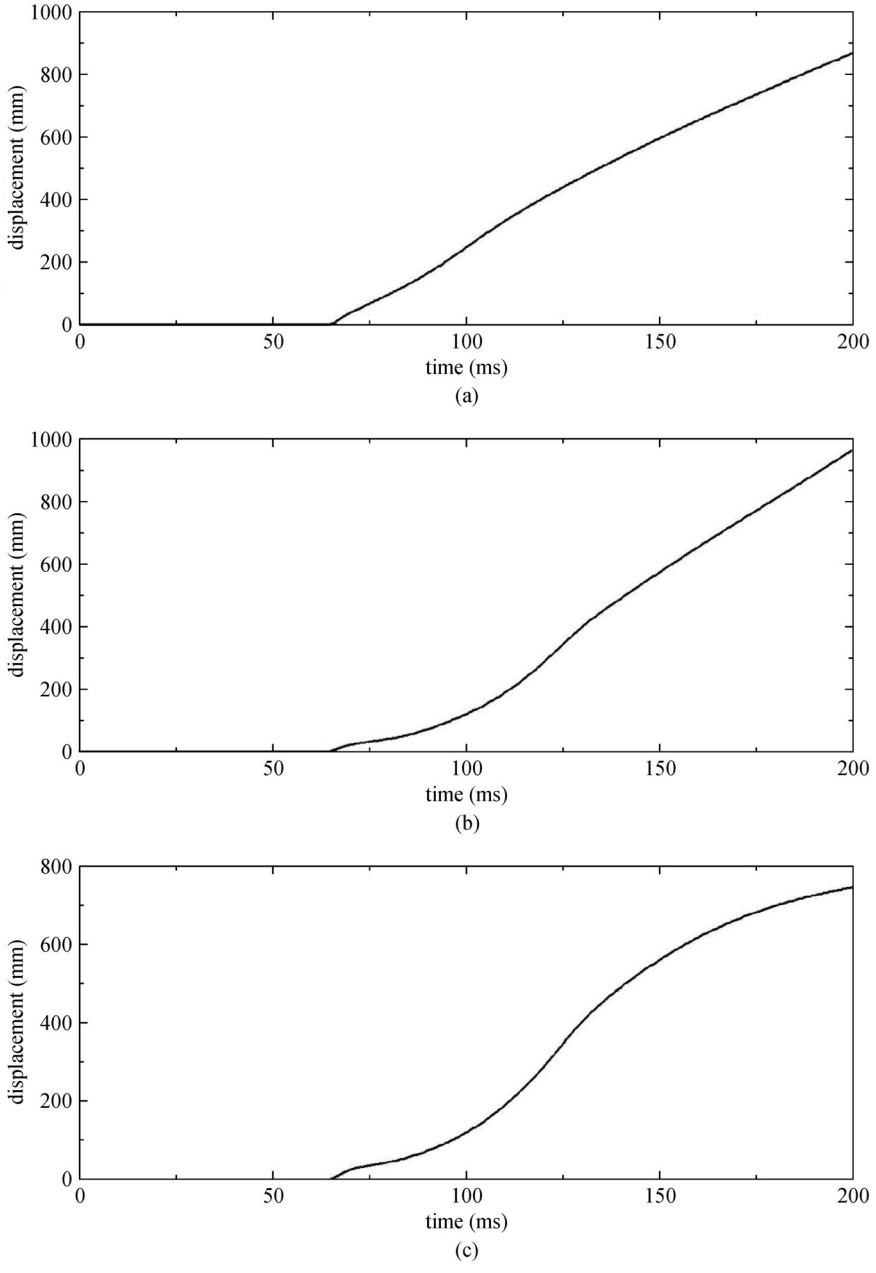

Fig. 20 Displacement plots for the RC column at (a) $Z = 0.6$ m/kg$^{1/3}$; (b) $Z = 0.8$ m/kg$^{1/3}$; (c) $Z = 1.0$ m/kg$^{1/3}$.

in the diameter of the longitudinal steel bar. The longitudinal reinforcement ratios in this study ranged from 0.011 to 0.028. Comparisons of the damage levels in the RC columns with different scaled distance and longitudinal reinforcement ratios are shown in Fig. 24. Besides the column depth, the reinforcement of the column could also have significant influence on the damage degree of RC columns.

This outcome indicates that with the increase of the longitudinal reinforcement ratio, damage degree decreases as the scaled distance increases. The increase in longitudinal reinforcement significantly enhances the bending strength of the column. The damage level of the RC columns increases by 26% when the longitudinal reinforcement ratio decreases from 0.028 to 0.011. The fitted polynomial graph and contour plot are then expressed in the form of surface plots to illustrate the damage degrees of RC columns with different longitudinal reinforcement

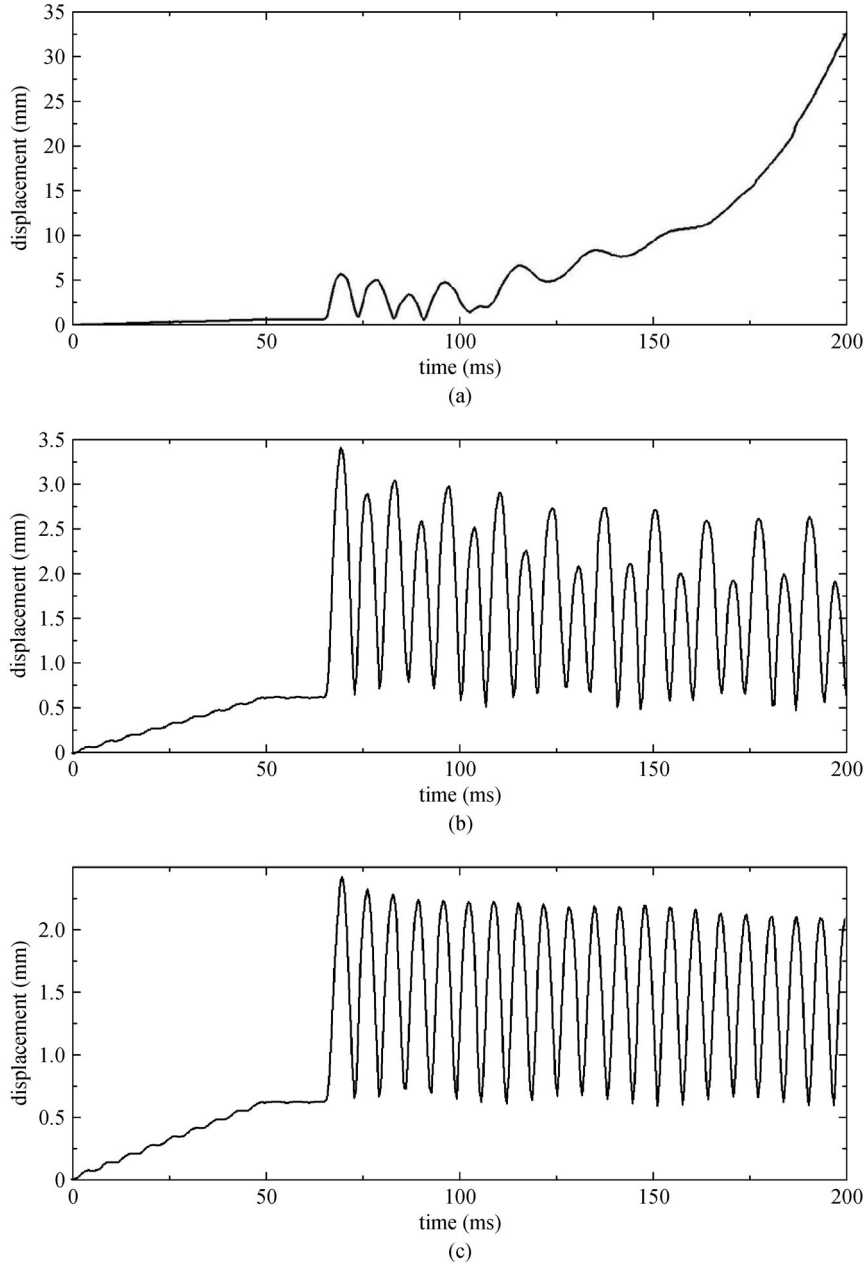

Fig. 21 Displacement plots for the RC column at (a) $Z = 1.5$ m/kg$^{1/3}$; (b) $Z = 2$ m/kg$^{1/3}$; (c) $Z = 2.5$ m/kg$^{1/3}$.

ratios under explosion loads is shown in Fig. 25, and the corresponding equation is given below.

$$D = -1.6916 + \left(\frac{1}{\rho}\right)^{0.032}(Z^{-0.573}). \quad (17)$$

6.4 Influence of charge weight on the residual capacity of RC columns with different concrete strength

In this section the effect of charge weight on residual axial load carrying capacity of the RC columns with different concrete strength was evaluated. The analysis to generate

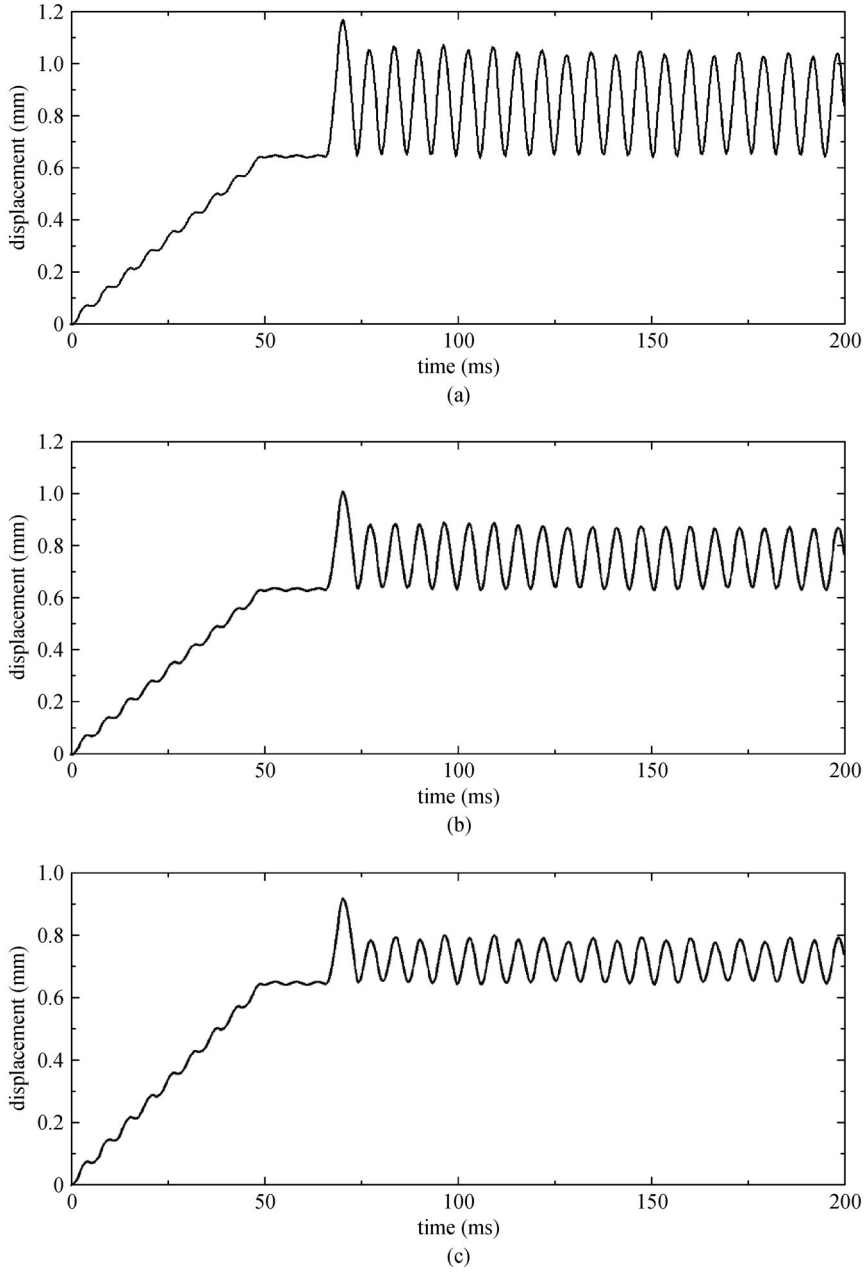

Fig. 22 Displacement plots for the RC column at (a) $Z = 4$ m/kg$^{1/3}$; (b) $Z = 4.5$ m/kg$^{1/3}$; (c) $Z = 5$ m/kg$^{1/3}$.

residual capacity of the RC columns consists of three stages: pre blast loading, blast loading, post blast loading stages. The axial load applied to the column in stage one and after that blast load is applied to the column after the time for stress equilibrium is attained along the length of the column in the stage two and in the third stage Post-blast analysis is carried out to evaluate the residual capacity of the column. This simulates a displacement controlled load testing. The concrete strength can have a significant affect in increasing the residual axial load carrying capacity of the RC columns under explosive loads. The concrete strength was varied between 32 and 52 MPa. Figure 26 shows the effect of concrete strength on the residual axial load carrying capacity of the RC columns. It can be seen that the concrete strength efficiency of residual axial load carrying capacity of RC columns increases with augmenting concrete strength. Generally, residual axial load carrying capacity of RC columns improves with increasing

Table 6 The range for charge weights and standoff distances at 0.95 m/kg$^{1/3}$ scaled distances

parameter	scaled distance (m/kg$^{1/3}$)	charge weight (kg)	standoff distance (m)
value	0.95	0.5	0.753
		5	1.62
		50	3.5
		597.2	8
		9330	20
		15000	23.58

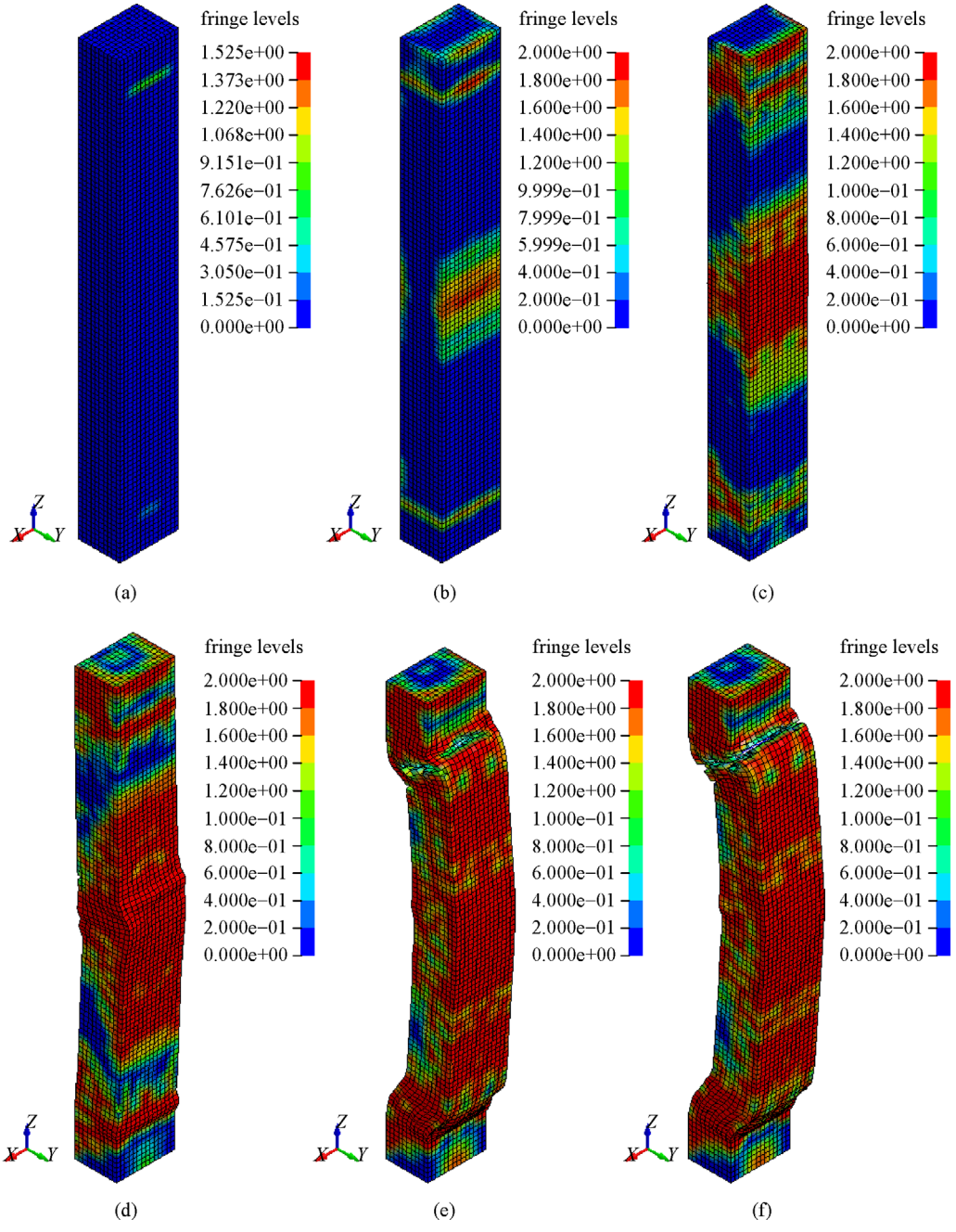

Fig. 23 Response of the RC column under same scaled distance. (a) $R = 0.753$ m, $W = 0.5$ kg; (b) $R = 1.62$ m, $W = 5$ kg; (c) $R = 3.5$ m, $W = 50$ kg; (d) $R = 8$ m, $W = 597.2$ kg; (e) $R = 20$ m, $W = 9330$ kg; (f) $R = 23.58$ m, $W = 15000$ kg.

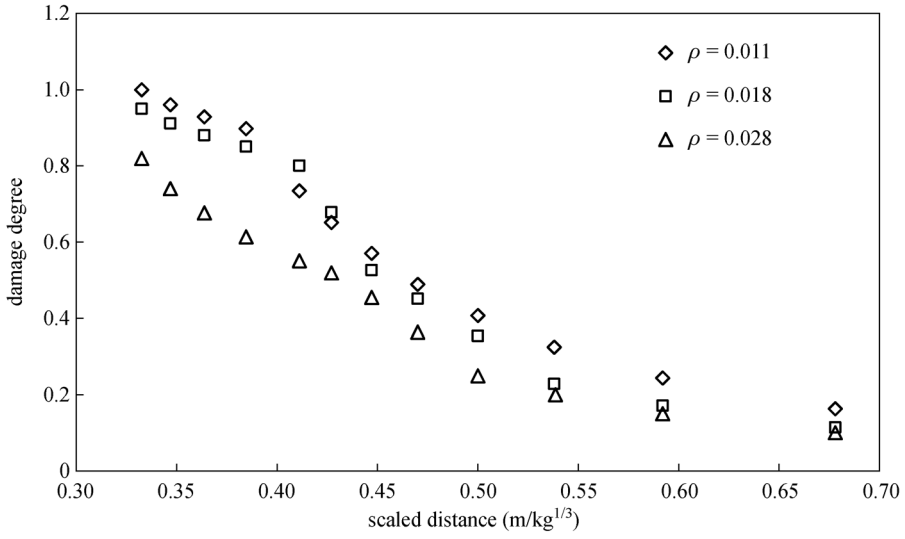

Fig. 24 Damage degree in RC columns with different ρ and Z.

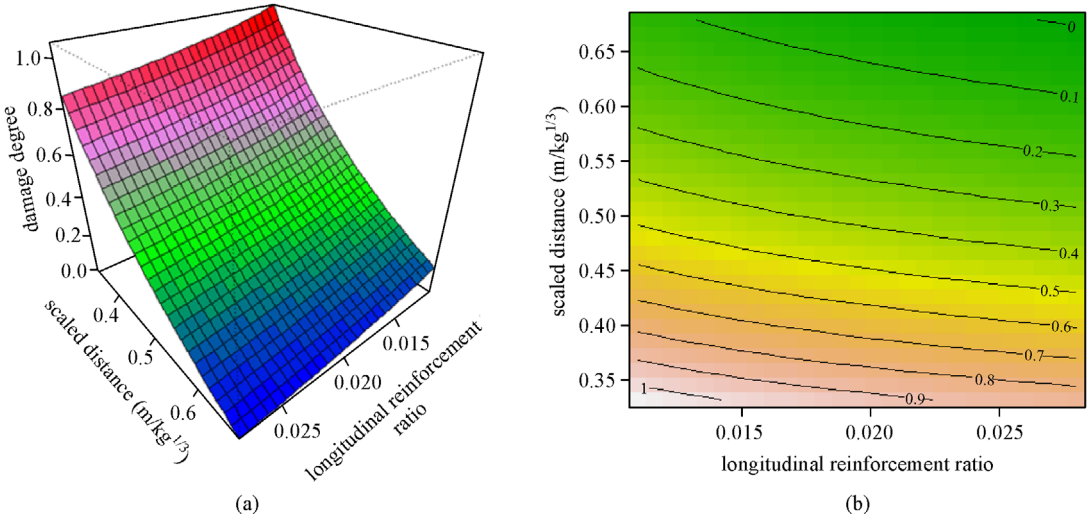

Fig. 25 (a) The best fitted curve, and (b) contour plot to predict the level of damage with different ρ.

concrete strength. The best fitted boundary surface and counter plot for the residual axial load carrying capacity of RC column with different concrete strength is shown in Fig. 27, and the corresponding equation is given below.

$$P_{\text{residual}} = 3046.85 + (f_{\text{c}}^{2.13})(W^{-1.02}), \qquad (18)$$

where P_{residual} is the residual axial load carrying capacity of RC column, f_{c} is the concrete strength and W is the charge weight.

6.5 Influence of charge weight on the residual capacity of RC columns with different width

The columns width range was taken between 500 and 900 mm to investigate the charge weight effect on the residual axial load carrying capacity of the RC columns under blast loads. Figure 28 shows the effect of column width on the residual capacity of the RC columns with various TNT charge weight. It can be seen that residual axial load carrying capacity of RC columns increase with the rise in column width. The results show that the residual axial load carrying capacity of RC column with low column width is significantly less than that of a column with high column width. The best fitted boundary surface and counter plot for the residual axial load carrying capacity of RC column with different width is shown in Fig. 29, and the corresponding equation is given below.

$$P_{\text{residual}} = 1307.17 + (w_i^{1.417})(W^{-0.792}), \qquad (19)$$

where P_{residual} is the residual axial load carrying capacity of

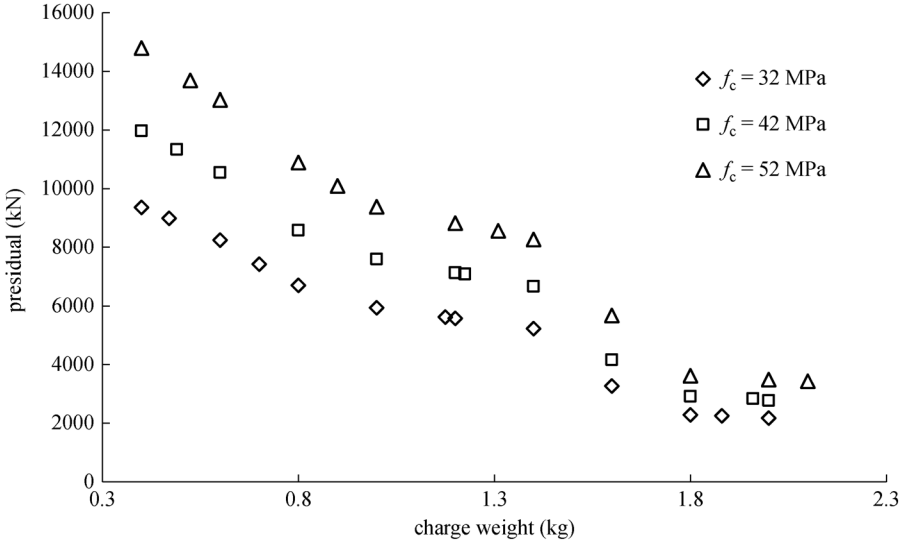

Fig. 26 Effects of concrete strength on the residual capacity of RC column with different charge weight.

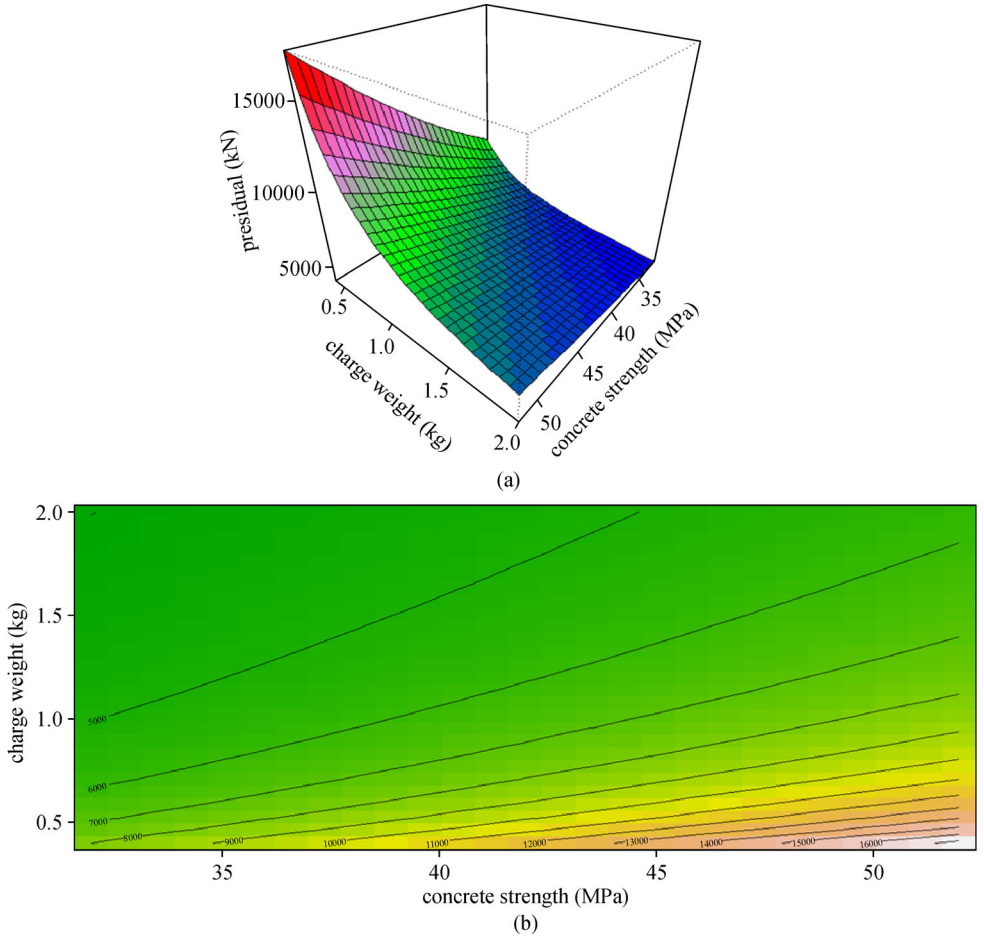

Fig. 27 (a) The best fitted curve and (b) counter fringe for the residual axial load carrying capacity of RC column with different concrete strength.

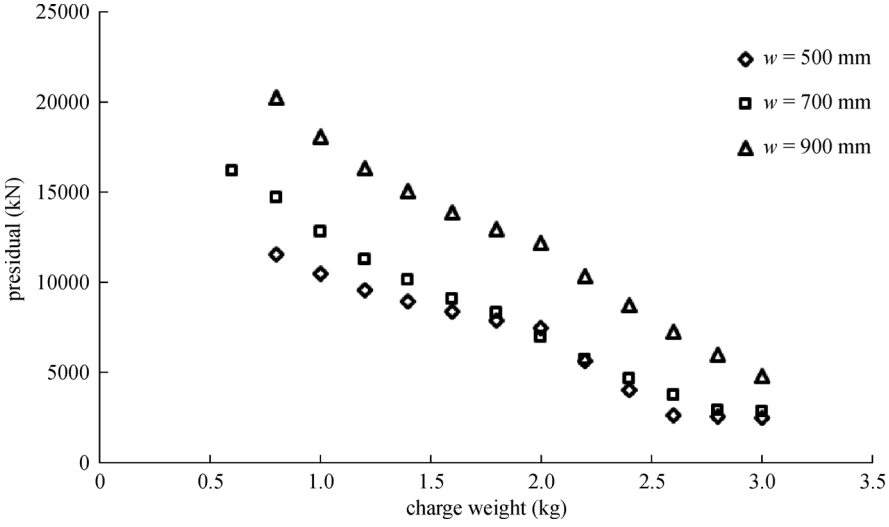

Fig. 28 Effects of column width on the residual axial load carrying capacity of RC column with different scaled distances.

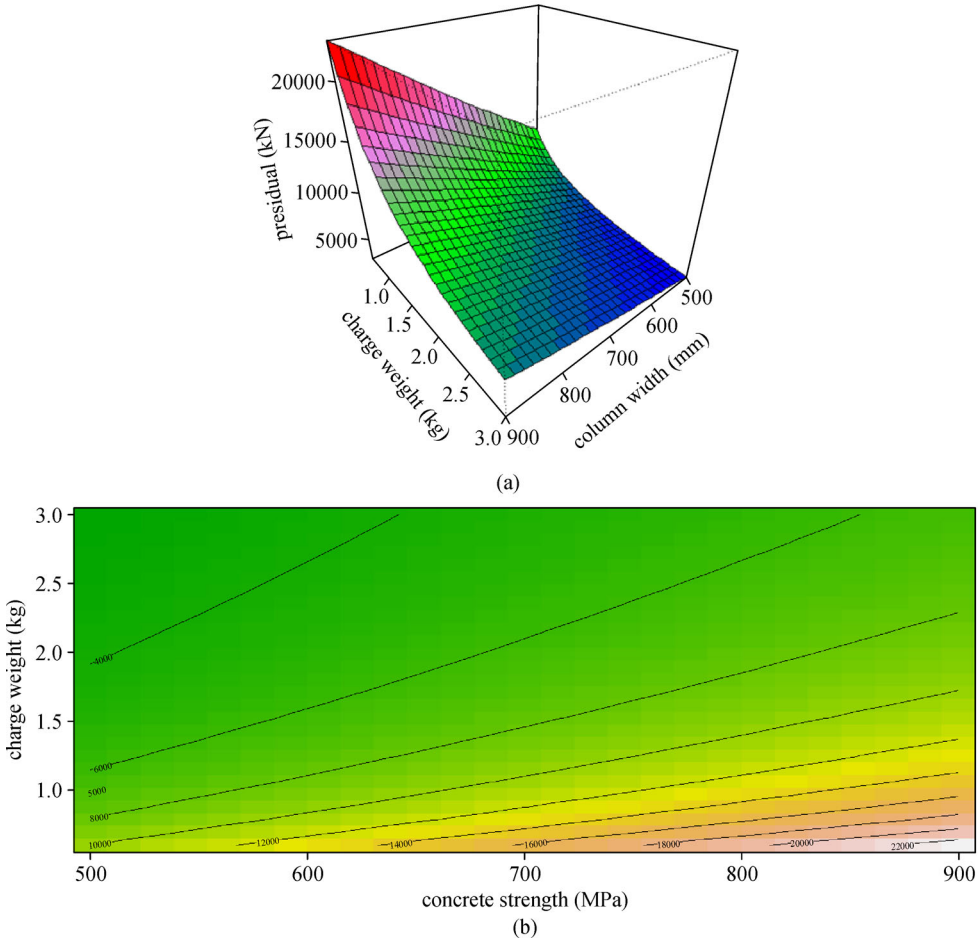

Fig. 29 (a) The best fitted curve and (b) counter fringe for the residual axial load carrying capacity of RC column with different columns width.

RC column, w_i is the column width and W is the charge weight.

7 Conclusions

In this research finite element analyses were performed to investigate the behavior of RC columns against blast detonations. The numerical simulations were validated against the blast field tests. The scaled distance was found a critical parameter to analyze the response of the RC column under explosive loads. The column experienced the maximum pressure and maximum impulse when the scaled distance was low. As a consequence, the column failed under intense impulsive regime loading. Also, results showed that higher scaled distant could decrease the damage level of RC column even further. Based on intensive numerical simulation data, analytical expressions are derived to predict damage degree and residual axial load carrying capacity of RC column in terms of the Scaled distance, charge weight, column width concrete strength and longitudinal reinforcement ratio. This research work and the conclusions drawn may be utilized for evaluation of the effect of an explosion on the RC column.

Acknowledgements The research was financially supported by the Ministry of Science and Technology of China (No. 2017YFC0703603), the Taishan Scholar Priority Discipline Talent Group program funded by the Shandong Province, and the Universiti Kebangsaan Malaysia Grant FRGS-1-2015-TK01-UKM02-4 and AP-2015-011.

References

1. Abedini M, Mutalib A A, Raman S N, Alipour R, Akhlaghi E. Pressure-impulse (P-I) diagrams for reinforced concrete (RC) structures: A review. Archives of Computational Methods in Engineering, 2019, 26: 733–767
2. Fertal M, Leone K. Applications of Blast/FX, an explosive effects analysis software tool. In: Proceedings IEEE 34th Annual 2000 International Carnahan Conference. Ottawa: IEEE, 2000, 218–221
3. Conrath E J. Structural design for physical security: State of the practice. American Society of Civil Engineers, 1999
4. Federal Emergency Management Agency (FEMA428). Explosive Blast. Washington: US department of Homeland Security, 2004
5. Morrill K, Malvar L, Crawford J, Ferritto J. Blast resistant design and retrofit of reinforced concrete columns and walls. In: Proceedings of the 2004 Structures Congress—Building on the Past: Securing the Future. Nashville: American Society of Civil Engineers, 2004, 1–8
6. Xu J, Wu C, Xiang H, Su Y, Li Z X, Fang Q, Hao H, Liu Z, Zhang Y, Li J. Behaviour of ultra high performance fibre reinforced concrete columns subjected to blast loading. Engineering Structures, 2016, 118: 97–107
7. Al-Thairy H. A modified single degree of freedom method for the analysis of building steel columns subjected to explosion induced blast load. International Journal of Impact Engineering, 2016, 94: 120–133
8. Zhang F, Wu C, Zhao X L, Heidarpour A, Li Z. Experimental and numerical study of blast resistance of square CFDST columns with steel-fibre reinforced concrete. Engineering Structures, 2017, 149: 50–63
9. Karlos V, Solomos G. Calculation of Blast Loads for Application to Structural Components. Luxembourg: Publications Office of the European Union, 2013
10. Alipour R, Izman S, Tamin M N. Estimation of Charge Mass for High Speed Forming of Circular Plates Using Energy Method. Advanced Materials Research, 2014, 845: 803–808
11. Abedini M, Mutalib A A. Investigation into damage criterion and failure modes of RC structures when subjected to extreme dynamic loads. Archives of Computational Methods in Engineering, 2020, 27: 501–515
12. Ngo T, Mendis P, Gupta A, Ramsay J. Blast loading and blast effects on structures—An overview. Electronic Journal of Structural Engineering, 2007, 7: 76–91
13. Almusallam T H, Elsanadedy H, Abbas H, Ngo T, Mendis P. Numerical analysis for progressive collapse potential of a typical framed concrete building. International Journal of Civil & Environmental Engineer, 2010, 10: 40–46
14. Remennikov A M. A review of methods for predicting bomb blast effects on buildings. Journal of Battlefield Technology, 2003, 6(3): 5–10
15. UFC-3-340-02. Design of structures to resist the effects of accidental explosions. US Army Corps of Engineers, Naval Facilities Engineering Command. Washington, D.C.: Air Force Civil Engineer Support Agency, Dept of the Army and Defense Special Weapons Agency, 2008.
16. Baylot J T, Bevins T L. Effect of responding and failing structural components on the airblast pressures and loads on and inside of the structure. Computers & Structures, 2007, 85(11–14): 891–910
17. Abedini M, Mutalib A A, Raman S N, Akhlaghi E, Mussa M H, Ansari M. Numerical investigation on the non-linear response of reinforced concrete (RC) columns subjected to extreme dynamic loads. Journal of Asian Scientific Research, 2017, 7(3): 86–98
18. LS-DYNA. Keyword User's Manual V971, CA: Livermore Software Technology Corporation (LSTC). Livermore, CA: LS-DYNA, 2015
19. Mussa M H, Mutalib A A, Hamid R, Naidu S R, Radzi N A M, Abedini M. Assessment of damage to an underground box tunnel by a surface explosion. Tunnelling and Underground Space Technology, 2017, 66: 64–76
20. Mutalib A A, Hao H. Development of P-I diagrams for FRP strengthened RC columns. International Journal of Impact Engineering, 2011, 38: 290–304
21. Malvar L J, Crawford J E, Wesevich J W, Simons D. A plasticity concrete material model for DYNA3D. International Journal of Impact Engineering, 1997, 19(9–10): 847–873
22. Soden P, Hinton M, Kaddour A. Lamina properties, lay-up configurations and loading conditions for a range of fibre-reinforced composite laminates. Composites Science and Technology, 1998, 58(7): 1011–1022
23. Mutalib A A, Hao H. Numerical analysis of FRP-composite-

strengthened RC panels with anchorages against blast loads. Journal of Performance of Constructed Facilities, 2011, 25(5): 360–372
24. Bobaru F, Mehrmashadi J, Chen Z, Niazi S. Intraply fracture in fiber-reinforced composites: A peridynamic analysis. In: The ASC 33rd Annual Technical Conference & 18th US-Japan Conference on Composite Materials. Seattle, 2018
25. Rabczuk T, Belytschko T. A three-dimensional large deformation meshfree method for arbitrary evolving cracks. Computer Methods in Applied Mechanics and Engineering, 2007, 196: 2777–2799
26. Rabczuk T, Belytschko T. Cracking particles: A simplified meshfree method for arbitrary evolving cracks. International Journal for Numerical Methods in Engineering, 2004, 61(13): 2316–2343
27. Wang B L, Guo Y B, Zhang C W. Cracking and thermal shock resistance of a Bi_2Te_3 based thermoelectric material. Engineering Fracture Mechanics, 2016, 152: 1–9
28. Zhang C W, Li L Y, Ou J P. Swinging motion control of suspended structures: Principles and applications. Structural Control and Health Monitoring, 2010, 17(5): 549–562
29. Behzadinasab M, Vogler T J, Peterson A M, Rahman R, Foster J T. Peridynamics modeling of a shock wave perturbation decay experiment in granular materials with intra-granular fracture. Journal of Dynamic Behavior of Materials, 2018, 4(4): 529–542
30. Mehrmashhadi J, Tang Y, Zhao X, Xu Z, Pan J J, Le Q V, Bobaru F. The effect of solder joint microstructure on the drop test failure—A peridynamic analysis. IEEE Transactions on Components, Packaging, and Manufacturing Technology, 2019, 9(1): 58–71
31. Watstein D. Effect of straining rate on the compressive strength and elastic properties of concrete. Journal Proceedings, 1953, 49(4): 729–744
32. Jones P G, Richart F. The effect of testing speed on strength and elastic properties of concrete. Proceedings, 1936, 36: 380–392
33. Glanville W H, Grime G, Fox E N, Davies W W. An Investigation of the Stresses in Reinforced Concrete Piles During Driving. HM Stationery Office, 1938
34. Comit Euro-International du Beton (CEB). CEB-FIP model code 1990: Design code. Telford, 1993
35. Abedini M, Mutalib A A, Raman S N, Akhlaghi E. Modeling the effects of high strain rate loading on RC columns using Arbitrary Lagrangian Eulerian (ALE) technique. Revista Internacional de Métodos Numéricos para Cálculo y Diseño en Ingeniería, 2018, 34: 1–23
36. Abedini M, Mutalib A, Raman S, Baharom S, Nouri J. Prediction of residual axial load carrying capacity of reinforced concrete (RC) columns subjected to extreme dynamic loads. American Journal of Engineering and Applied Sciences, 2017, 10(2): 431–448
37. Mutalib A A, Mohd Tawil N, Baharom S, Abedini M. Failure probabilities of FRP strengthened RC column to blast loads. Jurnal Teknologi, 2013, 65(2): 135–141
38. Marsh K, Campbell J. The effect of strain rate on the post-yield flow of mild steel. Journal of the Mechanics and Physics of Solids, 1963, 11(1): 49–63
39. Alipour R, Frokhi Nejad A, Izman S, Tamin M. Computer aided design and analysis of conical forming dies subjected to blast load. Applied Mechanics and Materials, 2015, 735: 50–56
40. Malvar L J. Review of static and dynamic properties of steel reinforcing bars. ACI Materials Journal, 1998, 95(5): 609–616
41. Abedini M, Mutalib A A, Raman S N. PI diagram generation for reinforced concrete (RC) columns under high impulsive loads using ALE method. Journal of Asian Scientific Research, 2017, 7(7): 253–262
42. Spacone E, Limkatanyu S. Responses of reinforced concrete members including bond-slip effects. Structural Journal, 2000, 97: 831–839
43. Luccioni B M, López D E, Danesi R F. Bond-slip in reinforced concrete elements. Journal of Structural Engineering, 2005, 131(11): 1690–1698
44. Fanning P. Nonlinear models of reinforced and post-tensioned concrete beams. Electronic Journal of Structural Engineering, 2001, 1: 111–119
45. Tavárez F A. Simulation of Behavior of Composite Grid Reinforced Concrete Beams Using Explicit Finite Element Methods. Madison: University of Wisconsin-Madison, 2001
46. Abedini M, Mutalib A A, Baharom S, Hao H. Reliability analysis of PI diagram formula for RC column subjected to blast load. In: Proceedings of World Academy of Science, Engineering and Technology. Kuala Lumpur, 2013, 665
47. Mutalib A A, Abedini M, Baharom S, Hao H. Derivation of empirical formulae to predict pressure and impulsive asymptotes for PI diagrams of one-way RC panels. In: Proceedings of World Academy of Science, Engineering and Technology. Kuala Lumpur, 2013, 661
48. Mutalib A A, Hao H. The effect of anchorages on FRP strengthening of RC walls to resist blast loads. Applied Mechanics and Materials, 2011, 82: 497–502
49. TM5-1300. Structures to Resist the Effects of the Accidental Explosions. New Jersey: US Department of Army, Picatinny Arsenal, 1990
50. Smith S J, McCann D M, Kamara M E. Blast Resistant Design Guide for Reinforced Concrete Structures. Skokie: Portland Cement Association, 2009